

Anomalous thermal Hall effect and anomalous Nernst effect of CsV_3Sb_5

Xuebo Zhou,^{1,2} Hongxiong Liu,² Wei Wu,² Kun Jiang,^{2,3} Youguo Shi,²

Zheng Li,^{2,3,*} Yu Sui,^{1,4,†} Jiangping Hu,^{2,3} and Jianlin Luo^{2,3,5,‡}

¹*School of Physics, Harbin Institute of Technology, Harbin 150001, China*

²*Beijing National Laboratory for Condensed Matter Physics and Institute of Physics,
Chinese Academy of Sciences, Beijing 100190, China*

³*School of Physical Sciences, University of Chinese
Academy of Sciences, Beijing 100190, China*

⁴*Laboratory for Space Environment and Physical Sciences,
Harbin Institute of Technology, Harbin 150001, China*

⁵*Songshan Lake Materials Laboratory, Dongguan 523808, China*

Abstract

Motivated by time-reversal symmetry breaking and giant anomalous Hall effect in kagome superconductor AV_3Sb_5 ($A = Cs, K, Rb$), we carried out the thermal transport measurements on CsV_3Sb_5 . In addition to the anomalous Hall effect, the anomalous Nernst effect and the anomalous thermal Hall effect emerge. Interestingly, the longitudinal thermal conductivity κ_{xx} largely deviates from the electronic contribution obtained from the longitudinal conductivity σ_{xx} by the Wiedemann-Franz law. In contrast, the thermal Hall conductivity κ_{xy} is roughly consistent with the Wiedemann-Franz law from electronic contribution. All these results indicate the large phonon contribution in the longitudinal thermal conductivity. Moreover, the thermal Hall conductivity is also slightly greater than the theoretical electronic contribution, indicating other charge neutral contributions. More than that, the Nernst coefficient and Hall resistivity show the multi-band behavior with possible additional contribution from Berry curvature at the low fields.

I. INTRODUCTION

The newly discovered kagome topological metal AV_3Sb_5 ($A = K, Rb, Cs$) has been found to be the first quasi-two-dimensional kagome superconductor, which becomes another platform to investigate the interplay of topology, electron correlation effects, and superconductivity [1–5]. However, whether this superconductor is unconventional owing to electron-electron correlation or conventional because of electron-phonon coupling is still under debate. From the unconventional side, both the V-shape tunneling density of states [6] and the zero-temperature residual thermal conductivity [7] have been reported. And recent low-temperature scanning tunneling microscopy (STM) resolved an unconventional pair density wave [8]. In contrast, nuclear magnetic resonance (NMR) measurements clearly reveal the spin singlet nature and point to a conventional s -wave superconductor from the Hebel-Slichter coherence peak [9]. This nodeless property is also consistent with penetration depth measurement [10] and impurity scattering feature from STM [11]. Additionally, high resolution angle-resolved photoemission spectroscopy (ARPES) finds the weakly correlated nature of AV_3Sb_5 and remarkable electron-phonon coupling [12].

* lizheng@iphy.ac.cn

† suiyu@hit.edu.cn

‡ jlluo@iphy.ac.cn

Besides superconductivity, the charge density wave (CDW) order in this nonmagnetic AV_3Sb_5 seems to be more unconventional. Several time-reversal symmetry-breaking signals have been found [13–15], especially the internal magnetic field induced relaxation rates in muon spin rotation (μ SR) [16]. AV_3Sb_5 also shows a giant anomalous Hall effect (AHE), which can be attributed to the enhanced skew scattering in the CDW state and the large Berry curvature from the kagome lattice and time-reversal symmetry breaking [17–20]. This AHE is concurrent with the CDW, indicating a strong correlation between CDW and AHE. As the thermoelectric counterpart and thermal counterpart of anomalous Hall effect, anomalous Nernst effect (ANE), and anomalous thermal Hall effect (ATHE) also play an important role in understanding quantum materials [21–24]. When the longitudinal heat flow in a magnetic field, the thermal Hall effect generates a transverse temperature gradient and the Nernst effect generates a transverse electric field, as illustrated in Fig. 1 (a). Normally, the Wiedemann-Franz (WF) law establishes a direct connection between electronic transport and electronic thermal transport [25, 26]. However, unlike the charge transport, other charge neutral excitations (e.g., phonons) can also contribute to the thermal transport. And the thermal Hall effect has been applied to probe topologically nontrivial excitations in insulators [27–29]. Hence, thermal transport provides a unique way toward identifying excitations and their topological properties.

In this work, we conducted extensive researches on the thermal transport properties of CsV_3Sb_5 , especially the anomalous thermal Hall and the anomalous Nernst effect. Interestingly, we found that the longitudinal thermal conductivity κ_{xx} largely deviates the electronic thermal conductivity contribution down to 5 K. It indicates the charge neutral excitation contribution to the thermal transport. However, the thermal Hall conductivity is more or less consistent with the Hall conductivity according to WF law. Since phonons normally do not contribute to the thermal Hall, κ_{xx} must contain a large phonon part down to low temperature. At low temperature, the thermal Hall conductivity is still slightly higher than the theoretical value $L_0\sigma_{xy}T$, indicating that the thermal Hall effect may have phonon-drag mechanism or other electrically neutral low energy excitation [30–33]. Additionally, we found the Nernst coefficient reaches a maximum value when the Hall resistivity is zero in the high magnetic field. This is the characteristic of ambipolar transport due to the multiband nature of CsV_3Sb_5 . However, this relationship no longer holds as the magnetic field decreases. Hence, there are other factors that dominate the transport properties at the low magnetic

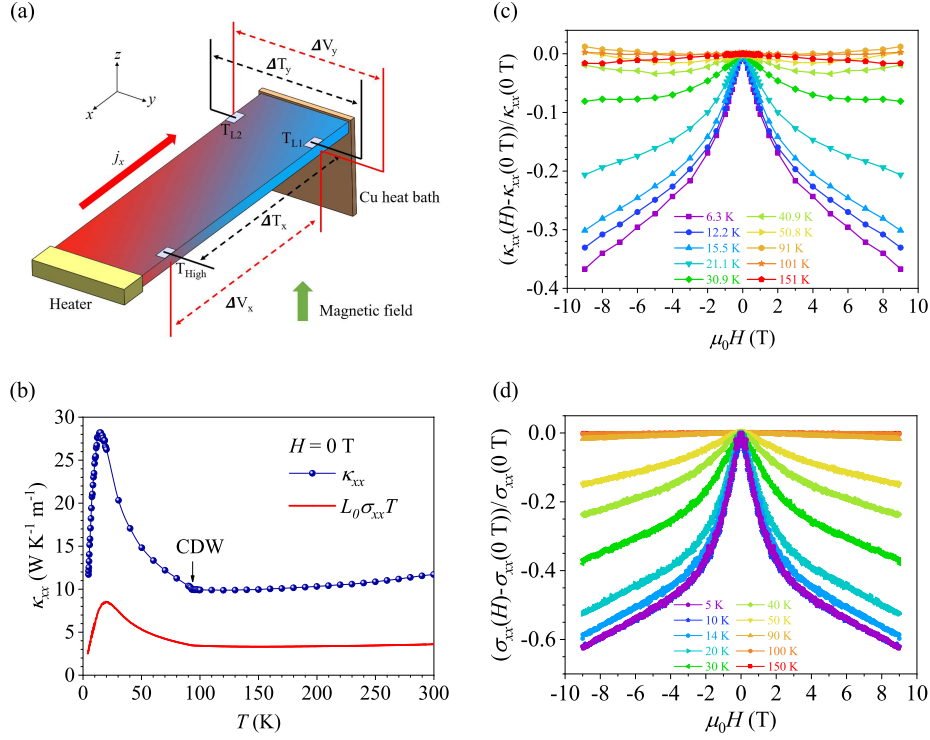


FIG. 1. (a) Schematic diagram of experimental setup. (b) Temperature dependence of longitudinal thermal conductivity κ_{xx} . The red curve is the electronic thermal conductivity calculated according to the WF law. Its value is smaller than the total thermal conductivity, which indicates that the phonons play an important role in thermal transportation. (c) Magnetic field dependence of longitudinal thermal conductivity κ_{xx} . (d) Magnetic field dependence of electrical conductivity σ_{xx} . Above 40 K, the dependence of σ_{xx} on magnetic field is weak, while below 40 K, σ_{xx} decreases rapidly with the field increasing.

field. The Berry curvature may contribute to the anomalous transverse response in the low field in addition to the multiband effect [26, 34].

II. EXPERIMENTAL DETAILS

High-quality CsV_3Sb_5 single crystals are prepared by a two-step self-flux method [1]. The thermal and electrical transport measurements were performed in a 9-T Quantum Design physical property measurement system. Schematic diagram of the experimental setup is shown in Fig. 1 (a). The sample is processed into a square piece. A resistance heater is used

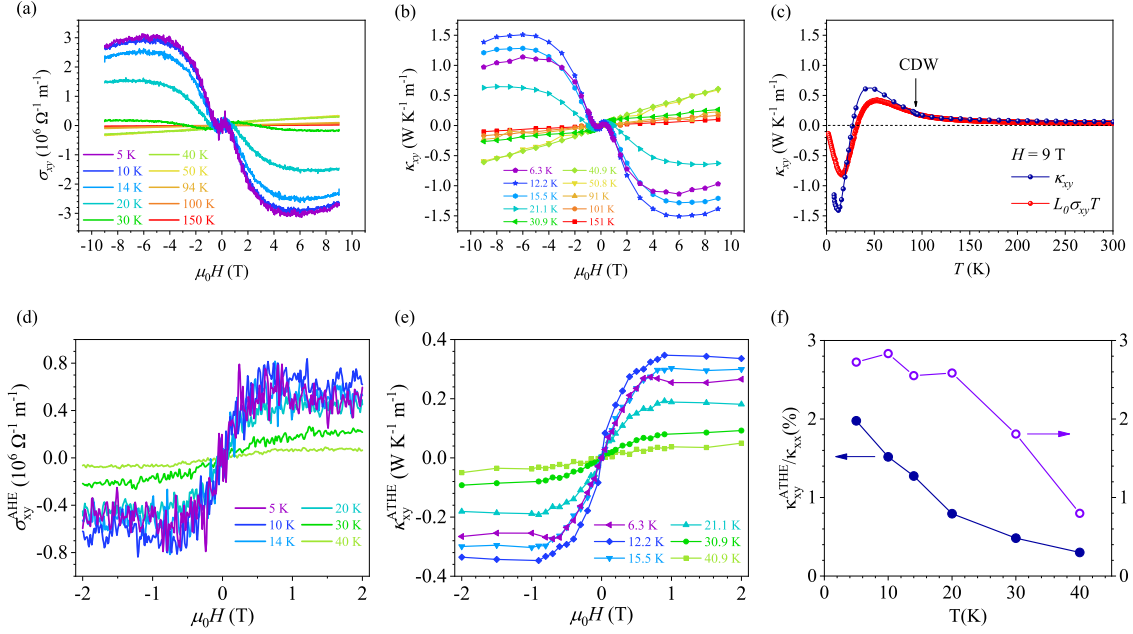


FIG. 2. (a) Magnetic field dependence of electrical Hall conductivity σ_{xy} . An appreciable antisymmetric side “S” line pattern appears in the low magnetic field region below 40 K. (b) Magnetic field dependence of thermal Hall conductivity κ_{xy} . An antisymmetric side “S” line pattern appears in the low magnetic field region below 40 K. (c) Temperature dependence of thermal Hall conductivity κ_{xy} . The red curve is the electronic thermal Hall conductivity calculated according to the WF law. (d) The extracted anomalous Hall conductivity at various temperatures. (e) The extracted anomalous thermal Hall conductivity at various temperatures. (f) Temperature dependence of anomalous thermal Hall ratio and anomalous Hall ratio in 2 T magnetic field

to generate a heat current $j_x = P/(Wd)$ in the plane, where P , W , and d are the heater power and the width and the thickness of the sample, respectively. The longitudinal voltage ΔV_x and the transverse voltage ΔV_y are measured by a Keithley 2182A nanovoltmeter. The longitudinal and transverse temperature gradients $\Delta T_x/l$ and $\Delta T_y/w$ were measured with field-calibrated chromel-AuFe_{0.07%} thermocouples, where l is the distance between the thermal contacts for T_{High} and T_{L1} and w is the distance between the thermal contacts for T_{L1} and T_{L2} . The longitudinal thermal conductivity is measured by $\kappa_{xx} = j_x l / \Delta T_x$ and the thermal Hall conductivity is measured by $\kappa_{xy} = -\kappa_{xx} [(\Delta T_y l) / (\Delta T_x w)]$. In order to eliminate the misalignment effect of thermocouple, $\Delta V_y(H) = [\Delta V_y(+H) - \Delta V_y(-H)]/2$

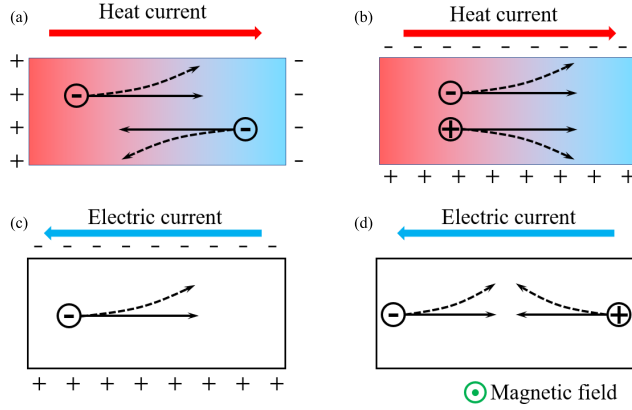


FIG. 3. [(a), (b)] Schematic diagram of the Nernst effect for a single-band metal and an ambipolar metal, respectively. In the single-band metal, the transverse charge current produced by the thermal gradient and electric field in a magnetic field will gather at both ends, so it will not produce a transverse electric field. However, in the ambipolar metal, the holes and the electrons will move toward the cold end under the drive of the thermal gradient and accumulate to both transverse ends in the magnetic field to produce a limited electric field. [(c), (d)] Schematic diagram of the Hall effect for a single-band metal and an ambipolar metal, respectively. In the ambipolar metal, the holes and the electrons moving in opposite direction will accumulate to the same transverse end under the magnetic field, resulting in cancellation of the transverse electric field. It means that the Nernst coefficient will appear a maximum value when the Hall effect is completely offset.

and $\Delta T_y(H) = [\Delta T_y(+H) - \Delta T_y(-H)]/2$ are obtained by subtracting the measurement results of the positive and negative fields, where H is the magnetic field perpendicular to the plane. Nernst coefficient N is calculated by $N = (\Delta V_y l) / (\Delta T_x w)$ and its sign is defined by using the vortex convention.

III. RESULT AND DISCUSSIONS

The electrical conductivity tensor $\bar{\sigma}$, thermal conductivity tensor $\bar{\kappa}$, and thermoelectric conductivity tensor $\bar{\alpha}$ relate the charge current \mathbf{J}_e and the heat current \mathbf{J}_q to the electric field \mathbf{E} and the thermal gradient ∇T [35]:

$$\begin{pmatrix} \mathbf{J}_e \\ \mathbf{J}_q \end{pmatrix} = \begin{pmatrix} \bar{\sigma} & -\bar{\alpha} \\ T\bar{\alpha} & -\bar{\kappa} \end{pmatrix} \begin{pmatrix} \mathbf{E} \\ \nabla T \end{pmatrix} \quad (1)$$

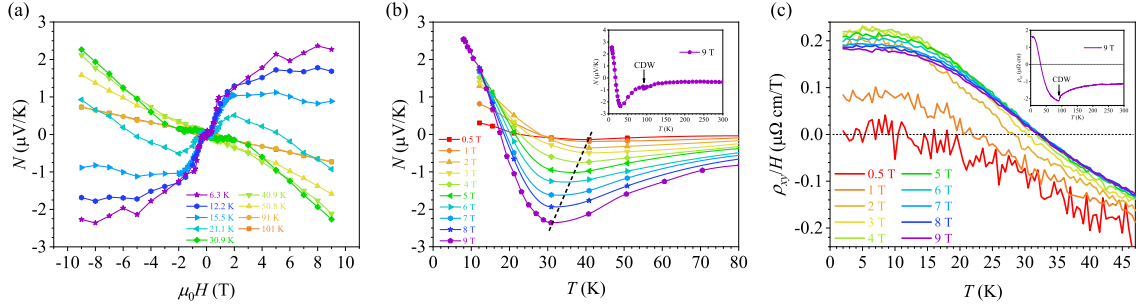


FIG. 4. (a) Magnetic field dependence of Nernst coefficient. The Nernst coefficient exhibits a linear magnetic field-dependent behavior above T_{CDW} . (b) Temperature dependence of Nernst coefficient. The Nernst coefficient shows an extreme value, which is marked by a dashed line. The temperature of the extreme value decreases as the magnetic field increases. (c) Temperature dependence of Hall resistivity divided by magnetic field. The compensation temperature of the Hall resistivity increases as the magnetic field increases.

Electrons contribute to both electrical and thermal conductivity in metals, so $\bar{\sigma}$ relate to $\bar{\kappa}$ by the WF law, $\kappa_e = L_0 \sigma T$. κ_e is the thermal conductivity of electrons and L_0 is Lorentz constant, $L_0 \equiv \frac{\pi^2 k_B^2}{3 e^2} = 2.44 \times 10^{-8} \text{ W}\Omega\text{K}^{-2}$. $\bar{\sigma}$ can be measured by applying charge current without thermal gradient ($\nabla T = 0$). $\bar{\alpha}$ and $\bar{\kappa}$ can be measured by applying heat current without charge current ($\mathbf{J}_e = 0$). Using the configuration shown in Fig. 1 (a), we measured the longitudinal thermal conductivity, the thermal Hall conductivity, the electrical hall conductivity, and the Nernst coefficient.

The temperature dependence of the longitudinal thermal conductivity κ_{xx} is shown in Fig. 1 (b). Above T_{CDW} , κ_{xx} decreases with decreasing temperature, which is different from ordinary materials, indicating that CDW fluctuations have a strong scattering effect on electron and phonon transport. In the CDW order state, charge fluctuations are suppressed and the mean free path of electrons and phonons increases, so κ_{xx} increases rapidly below T_{CDW} until it reaches a peak. The total thermal conductivity is contributed by both phonons and electrons, $\kappa = \kappa_e + \kappa_{\text{ph}}$, where κ_e is the electron thermal conductivity and κ_{ph} is the phonon thermal conductivity [36]. In metals with short mean free path, the thermal conductivity of phonons should be of the same magnitude as that of electrons. In order to compare the relationship between electrical conductivity and thermal conductivity, we converted electrical conductivity into electronic thermal conductivity, $L_0 \sigma_{xx} T$, according

to the WF law, as shown in Fig. 1 (b). The total thermal conductivity is greater than $L_0\sigma_{xx}T$. The difference is due to the phonon contribution, which is of the same magnitude as the electron contribution, indicating that phonons play an important role in the thermal transport. The thermal conductivity may also involve the influence of electron fluctuations on phonon scattering before and after CDW. The electron fluctuations near CDW phase transition will enhance the phonon scattering, and the thermal conductivity of phonon is suppressed. So, the thermal conductivity increases slightly with the increase of temperature at 100 – 300 K. As a result, WF law does not recover at 300 K, and may recover at a higher temperature [36–40].

The magnetic field dependence of longitudinal thermal conductivity κ_{xx} and electrical conductivity σ_{xx} at various temperatures are shown in Figs. 1 (c) and 1 (d) respectively. Above 40 K, the field dependence of κ_{xx} and electrical conductivity σ_{xx} are weak, while below 40 K, the field dependence of κ_{xx} and electrical conductivity σ_{xx} become strong. The field dependence of longitudinal thermal conductivity is weaker than that of electronic conductivity, which also indicates the contribution of phonons to thermal transport.

Phonon thermal conductivity generally has no transverse effect, so the transverse thermal conductivity, namely thermal Hall conductivity, is a good method to study the thermal transport properties of electron. Figures 2 (a) and 2 (b) show the field dependence of electrical Hall conductivity σ_{xy} and thermal Hall conductivity κ_{xy} . Both σ_{xy} and κ_{xy} show linear field-dependent behaviors as conventional metals above T_{CDW} . Between T_{CDW} and 40 K, κ_{xy} is still linear magnetic field dependent in the high field region, but weakly nonlinear in the low field region. Below 40 K, anomalous behaviors of thermal Hall conductivity arise. This anomalous behavior near 40 K is close related to the similar behaviors found in the muon spin relaxation rate, coherent phonon spectroscopy and Raman spectroscopy [41–43], which have been recently proved to be an electronic nematic transition [44]. Below 30 K, there are two antisymmetric sideways “S” shape, as shown in Figs. 2 (a) and 2 (b). They exist in the high and low fields respectively. The antisymmetric sideways “S” shape is a characteristic of either an AHE or a two-band ordinary Hall effect. When the temperature rises above 30 K, the S-shaped hump in the high field disappears and changes linearly with the magnetic field, but the S-shaped hump in the low field still exists. It implies that the S-shape hump in the high field is the result of the two-band effect, and the S-shaped hump in the low field is related to ATHE [17, 18]. We extract anomalous Hall conductivity σ_{xy}^{AHE} and

anomalous thermal Hall conductivity $\kappa_{xy}^{\text{ATHE}}$ by subtracting a local linear ordinary electrical Hall and thermal Hall background, as shown in Figs. 2 (d) and 2 (e). The anomalous thermal Hall conductivity $\kappa_{xy}^{\text{ATHE}}$ increases rapidly with the magnetic field in the low field (below 1 T) and saturates above 1 T. The saturation value of $0.35 \text{ WK}^{-1}\text{m}^{-1}$ is in the range for metals with anomalous Hall effect and close to Co_2MnGa [25, 26, 45]. The anomalous thermal Hall ratio is comparable to that of anomalous Hall ratio (AHR) in 2 T magnetic field, as shown in Fig. 2 (f), which is larger than the AHR of Fe, $\sim 0.8\%$ [46]. Anomalous Hall effect has been found in AV_3Sb_5 in previous studies on electric transport. By extracting σ_{AHE} at different angles of magnetic field relative to applied current, it is found that σ_{AHE} is not linearly proportional to the magnetic field component out of plane, which confirms the existence of AHE in AV_3Sb_5 . For the kagome metal AV_3Sb_5 AHE, the current mainstream view is that AHE originates from the skew scattering effect [17, 18] and Berry curvature [18, 47]. The kagome sublattice in AV_3Sb_5 acts as a tilted spin cluster, which results in the enhancement of the skew scattering effect. In addition, AV_3Sb_5 has a large Berry curvature due to kagome lattice and its topological properties, which may be related to AHE.

Figure 2 (c) shows the temperature dependence of κ_{xy} at 9 T. The thermal Hall effect is relatively weak at high temperature and becomes obvious with cooling. As the temperature decreases, κ_{xy} increases first and reaches a maximum around 40 K, which happens to be the temperature at which anomalous behaviors begin to appear. As the temperature decreases further, κ_{xy} changes sign at 27 K, and reaches another extreme value at 12.5 K. In order to compare the thermal Hall conductivity and the electrical Hall conductivity, we calculate the electronic thermal Hall conductivity contribution $L_0\sigma_{xy}T$ by using the WF law, as shown in Fig. 2 (c). The behavior of κ_{xy} is similar to $L_0\sigma_{xy}T$, but the value is slightly larger than $L_0\sigma_{xy}T$. Phonons, as neutral quasiparticles with no charge, should not directly produce thermal Hall effect. It implies that phonon-drag mechanism or electronically neutral topological low energy excitation may exist in the thermal Hall effect of the system [48]. Combined with the large phonon contribution in κ_{xx} , a strong electron-phonon coupling in CsV_3Sb_5 was observed from our thermal measurements. Since the superconductivity is one of the most important properties in the AV_3Sb_5 materials, what is the driving force for SC becomes one central issue. The electron-phonon coupling observed here further supports the superconductivity of CsV_3Sb_5 is a conventional s wave [9–12].

In order to further study the anomalous transverse effect, we carried out the Nernst effect

measurement. Equation (1) yields

$$\mathbf{E} = \bar{\sigma}^{-1} \bar{\alpha} \nabla T \quad (2)$$

For a single band metal, the Nernst coefficient derived from Eq. (2) is

$$N = \frac{E_y}{\nabla_x T} = \frac{\alpha_{xy} \sigma_{xx} - \alpha_{xx} \sigma_{xy}}{\sigma_{xx}^2 + \sigma_{xy}^2} \quad (3)$$

If the electric conductivity does not depend on energy, then

$$\frac{\sigma_{xy}}{\sigma_{xx}} = \frac{\alpha_{xy}}{\alpha_{xx}} \quad (4)$$

Therefore, the two terms in Eq. (3) are eliminated, which is called ‘‘Sondheimer cancellation.’’ As shown in Fig. 3 (a), the charge current generated by the thermal gradient will accumulate charges and create an electric field. The charge current produced by the thermal gradient and electric field offsets each other. However, this cancellation does not affect the electrical Hall effect. On the other hand, ambipolar flow can lead to an enhancement of the Nernst signal in multiband metals [35, 49]. If we assume two types of carriers, Eq. (3) is rewritten as

$$N = \frac{(\alpha_{xy}^+ + \alpha_{xy}^-)(\sigma_{xx}^+ + \sigma_{xx}^-) - (\alpha_{xx}^+ + \alpha_{xx}^-)(\sigma_{xy}^+ + \sigma_{xy}^-)}{(\sigma_{xx}^+ + \sigma_{xx}^-)^2 + (\sigma_{xy}^+ + \sigma_{xy}^-)^2} \quad (5)$$

The superscripts + and – indicate the hole-like and the electron-like carriers. The σ_{xy} of two type carries have opposite signs, so the Sondheimer cancellation is avoid. Especially when $\sigma_{xy}^- = -\sigma_{xy}^+$, Eq. (5) has a maximum, which means that the Nernst coefficient will show a maximum when the Hall effect is suppressed, as shown in Fig. 3.

The field dependence of Nernst coefficient N in CsV_3Sb_5 at various temperatures is shown in Fig. 4 (a). Similar to Hall resistivity, the Nernst coefficient exhibits linear field-dependent behavior above T_{CDW} . When the temperature is lower than T_{CDW} , the Nernst coefficient gradually deviates from the linear magnetic field dependence and the anomalous behavior show up below 40 K. The temperature variation of Nernst coefficient and Hall resistance in various magnetic fields are shown in Figs. 4 (b) and 4 (c) respectively. At 9 T, the Nernst coefficient reaches its maximum value at 32 K where $\rho_{xy} = 0$, which indicates a multiband effect. When the magnetic field decreases, the temperature of the extreme value of Nernst coefficient increases and reaches 40 K at zero field limit, while the compensation temperature of Hall resistivity decreases and approaches zero at zero field limit. Hence, there are other factors that influence the transport properties. Nernst and Hall signals are dominated

by normal linear items in high magnetic fields and dominated by anomalous items in low magnetic fields. Therefore, the multiband model should not be the only reason for the relationship between Hall resistivity and Nernst coefficient in low magnetic fields. One possible reason is that a new small electronic pocket with high mobility appears under CDW [35, 50]. But there is no direct experimental evidence for the new small electronic pocket with high mobility after CDW phase transition in AV_3Sb_5 , which can be seen from the high-resolution ARPES measurements. [2, 12, 51–54]. In the anomalous Hall effect studies of AV_3Sb_5 [17, 18], the skew scattering has been widely proposed. However, since the skew scattering does not break Sondheimer cancellation, the finite Nernst signal in low fields should be dominated by other origins, like the Berry curvature from the Z_2 topological property and time-reversal symmetry breaking in CsV_3Sb_5 [22, 55]. The expressions of anomalous Hall conductivity σ_{ij} and anomalous thermal Hall conductivity κ_{ij} can be obtained according to theoretical derivation [26, 56]:

$$\sigma_{ij}^A(\mu) = \frac{e^2}{\hbar} \int_{-\infty}^{\infty} d\xi \left(-\frac{\partial f(\xi - \mu)}{\partial \xi} \right) \tilde{\sigma}_{ij}(\xi) \quad (6)$$

$$\kappa_{ij}^A(\mu) = \frac{1}{\hbar T} \int_{-\infty}^{\infty} d\xi \left(-(\xi - \mu)^2 \frac{\partial f(\xi - \mu)}{\partial \xi} \right) \tilde{\sigma}_{ij}(\xi) \quad (7)$$

$$\tilde{\sigma}_{ij}(\xi) = \int_{\text{BZ}} \frac{d\mathbf{k}}{(2\pi)^3} \sum_{\epsilon_n < \xi} \Omega_{ij}^n(\mathbf{k}) \quad (8)$$

where $\Omega_{ij}^n(\mathbf{k})$ is Berry curvature and $f(\xi - \mu) = 1/(e^{(\xi - \mu)/k_B T} + 1)$ is the Fermi-Dirac function. From the comparison of Eqs. (6) and (7), we can find that the Berry curvature contributions to the thermal and electrical transport have different pondering functions, which leads to the mismatch between σ_{ij} and κ_{ij} [26, 57]. These differences reflect the fact that Berry curvatures from different regions of reciprocal space carry opposite signs and thus compete, which may cause the WF ratio to increase or decrease [56].

IV. SUMMARY

In summary, we performed the thermal transport measurements on CsV_3Sb_5 . Both the longitudinal thermal conductivity and the thermal Hall conductivity are larger than the theoretical values, indicating that there is a large phonon contribution in thermal transports. This shows that the phonon plays an important role in the physics of CsV_3Sb_5 even at low

temperature, which is consistent with the electron-phonon coupling found in ARPES [12] and a conventional s -wave superconductor from NMR [9] and penetration depth measurement [10]. The anomalous thermal Hall effect and the anomalous Nernst effect appear in the CDW state. The Nernst coefficient reaches a maximum value when the Hall resistivity is zero at 9 T, which indicates a multiband effect domination. As the magnetic field decreases, the maximum of Nernst effect shifts to higher temperature, while the zero value of Hall resistivity shifts to lower temperature. It indicates that the anomalous transverse response in the low field may have a contribution from the Berry curvature.

Note Added. During the preparation of this manuscript, we realized that a similar anomalous Nernst effect on CsV_3Sb_5 has been posted in Ref. [47], which is consistent with our results.

ACKNOWLEDGMENTS

This work was supported by the National Key Research and Development Program of China (Grant No. 2017YFA0302901), the National Science Foundation of China (Grants No. 12134018, No. 11921004, No. 11634015), the Strategic Priority Research Program and Key Research Program of Frontier Sciences of the Chinese Academy of Sciences (Grant No. XDB33010100), and the Synergetic Extreme Condition User Facility (SECUF).

-
- [1] B. R. Ortiz, L. C. Gomes, J. R. Morey, M. Winiarski, M. Bordelon, J. S. Mangum, I. W. H. Oswald, J. A. Rodriguez-Rivera, J. R. Neilson, S. D. Wilson, E. Ertekin, T. M. McQueen, and E. S. Toberer, New kagome prototype materials: discovery of KV_3Sb_5 , RbV_3Sb_5 , and CsV_3Sb_5 , *Phys. Rev. Materials* **3**, 094407 (2019).
 - [2] B. R. Ortiz, S. M. L. Teicher, Y. Hu, J. L. Zuo, P. M. Sarte, E. C. Schueller, A. M. M. Abeykoon, M. J. Krogstad, S. Rosenkranz, R. Osborn, R. Seshadri, L. Balents, J. He, and S. D. Wilson, CsV_3Sb_5 : A \mathbb{Z}_2 topological kagome metal with a superconducting ground state, *Phys. Rev. Lett.* **125**, 247002 (2020).
 - [3] B. R. Ortiz, P. M. Sarte, E. M. Kenney, M. J. Graf, S. M. L. Teicher, R. Seshadri, and S. D. Wilson, Superconductivity in the \mathbb{Z}_2 kagome metal KV_3Sb_5 ,

- Phys. Rev. Materials **5**, 034801 (2021).
- [4] Q. W. Yin, Z. J. Tu, C. S. Gong, Y. Fu, S. H. Yan, and H. C. Lei, Superconductivity and Normal-State Properties of Kagome Metal RbV_3Sb_5 Single Crystals, Chinese Physics Letters **38**, 6 (2021).
- [5] K. Jiang, T. Wu, J.-X. Yin, Z. Wang, M. Z. Hasan, S. D. Wilson, X. Chen, and J. Hu, Kagome superconductors AV_3Sb_5 ($A=\text{K, Rb, Cs}$) (2021), arXiv:2109.10809 [cond-mat.supr-con].
- [6] H. Zhao, H. Li, B. R. Ortiz, S. M. L. Teicher, T. Park, M. Ye, Z. Wang, L. Balents, S. D. Wilson, and I. Zeljkovic, Cascade of correlated electron states in a kagome superconductor CsV_3Sb_5 (2021), arXiv:2103.03118 [cond-mat.supr-con].
- [7] C. C. Zhao, L. S. Wang, W. Xia, Q. W. Yin, J. M. Ni, Y. Y. Huang, C. P. Tu, Z. C. Tao, Z. J. Tu, C. S. Gong, H. C. Lei, Y. F. Guo, X. F. Yang, and S. Y. Li, Nodal superconductivity and superconducting domes in the topological Kagome metal CsV_3Sb_5 (2021), arXiv:2102.08356 [cond-mat.supr-con].
- [8] H. Chen, H. Yang, B. Hu, Z. Zhao, J. Yuan, Y. Xing, G. Qian, Z. Huang, G. Li, Y. Ye, S. Ma, S. Ni, H. Zhang, Q. Yin, C. Gong, Z. Tu, H. Lei, H. Tan, S. Zhou, C. Shen, X. Dong, B. Yan, Z. Wang, and H.-J. Gao, Roton pair density wave in a strong-coupling kagome superconductor, Nature **599**, 222 (2021).
- [9] C. Mu, Q. Yin, Z. Tu, C. Gong, H. Lei, Z. Li, and J. Luo, S-Wave Superconductivity in Kagome Metal CsV_3Sb_5 Revealed by $^{121/123}\text{Sb}$ NQR and ^{51}V NMR Measurements, Chinese Physics Letters **38**, 077402 (2021).
- [10] W. Duan, Z. Nie, S. Luo, F. Yu, B. R. Ortiz, L. Yin, H. Su, F. Du, A. Wang, Y. Chen, X. Lu, J. Ying, S. D. Wilson, X. Chen, Y. Song, and H. Yuan, Nodeless superconductivity in the kagome metal CsV_3Sb_5 , Science China Physics, Mechanics & Astronomy **64**, 107462 (2021).
- [11] H.-S. Xu, Y.-J. Yan, R. Yin, W. Xia, S. Fang, Z. Chen, Y. Li, W. Yang, Y. Guo, and D.-L. Feng, Multiband Superconductivity with Sign-Preserving Order Parameter in Kagome Superconductor CsV_3Sb_5 , Phys. Rev. Lett. **127**, 187004 (2021).
- [12] H. Luo, Q. Gao, H. Liu, Y. Gu, D. Wu, C. Yi, J. Jia, S. Wu, X. Luo, Y. Xu, L. Zhao, Q. Wang, H. Mao, G. Liu, Z. Zhu, Y. Shi, K. Jiang, J. Hu, Z. Xu, and X. J. Zhou, Electronic nature of charge density wave and electron-phonon coupling in kagome superconductor KV_3Sb_5 , Nature Communications **13**, 273 (2022).
- [13] Y.-X. Jiang, J.-X. Yin, M. M. Denner, N. Shumiya, B. R. Ortiz, G. Xu, Z. Guguchia, J. He,

- M. S. Hossain, X. Liu, J. Ruff, L. Kautzsch, S. S. Zhang, G. Chang, I. Belopolski, Q. Zhang, T. A. Cochran, D. Multer, M. Litskevich, Z.-J. Cheng, X. P. Yang, Z. Wang, R. Thomale, T. Neupert, S. D. Wilson, and M. Z. Hasan, Unconventional chiral charge order in kagome superconductor KV_3Sb_5 , *Nature Materials* **20**, 1353 (2021).
- [14] N. Shumiya, M. S. Hossain, J.-X. Yin, Y.-X. Jiang, B. R. Ortiz, H. Liu, Y. Shi, Q. Yin, H. Lei, S. S. Zhang, G. Chang, Q. Zhang, T. A. Cochran, D. Multer, M. Litskevich, Z.-J. Cheng, X. P. Yang, Z. Guguchia, S. D. Wilson, and M. Z. Hasan, Intrinsic nature of chiral charge order in the kagome superconductor RbV_3Sb_5 , *Phys. Rev. B* **104**, 035131 (2021).
- [15] C. Mielke, D. Das, J.-X. Yin, H. Liu, R. Gupta, Y.-X. Jiang, M. Medarde, X. Wu, H. C. Lei, J. Chang, P. Dai, Q. Si, H. Miao, R. Thomale, T. Neupert, Y. Shi, R. Khasanov, M. Z. Hasan, H. Luetkens, and Z. Guguchia, Time-reversal symmetry-breaking charge order in a kagome superconductor, *Nature* **602**, 245 (2022).
- [16] L. Yu, C. Wang, Y. Zhang, M. Sander, S. Ni, Z. Lu, S. Ma, Z. Wang, Z. Zhao, H. Chen, K. Jiang, Y. Zhang, H. Yang, F. Zhou, X. Dong, S. L. Johnson, M. J. Graf, J. Hu, H.-J. Gao, and Z. Zhao, Evidence of a hidden flux phase in the topological kagome metal CsV_3Sb_5 (2021), arXiv:2107.10714 [cond-mat.supr-con].
- [17] S.-Y. Yang, Y. Wang, B. R. Ortiz, D. Liu, J. Gayles, E. Derunova, R. Gonzalez-Hernandez, L. Šmejkal, Y. Chen, S. S. P. Parkin, S. D. Wilson, E. S. Toberer, T. McQueen, and M. N. Ali, Giant, unconventional anomalous Hall effect in the metallic frustrated magnet candidate, KV_3Sb_5 , *Science Advances* **6**, eabb6003 (2020).
- [18] F. H. Yu, T. Wu, Z. Y. Wang, B. Lei, W. Z. Zhuo, J. J. Ying, and X. H. Chen, Concurrence of anomalous Hall effect and charge density wave in a superconducting topological kagome metal, *Phys. Rev. B* **104**, L041103 (2021).
- [19] N. Nagaosa, J. Sinova, S. Onoda, A. H. MacDonald, and N. P. Ong, Anomalous Hall effect, *Rev. Mod. Phys.* **82**, 1539 (2010).
- [20] D. Xiao, M.-C. Chang, and Q. Niu, Berry phase effects on electronic properties, *Rev. Mod. Phys.* **82**, 1959 (2010).
- [21] M. Li and G. Chen, Thermal transport for probing quantum materials, *MRS Bulletin* **45**, 348 (2020).
- [22] D. Xiao, Y. Yao, Z. Fang, and Q. Niu, Berry-phase effect in anomalous thermoelectric transport, *Phys. Rev. Lett.* **97**, 026603 (2006).

- [23] S. Onoda, N. Sugimoto, and N. Nagaosa, Quantum transport theory of anomalous electric, thermoelectric, and thermal Hall effects in ferromagnets, *Phys. Rev. B* **77**, 165103 (2008).
- [24] Y. Shiomi, Y. Onose, and Y. Tokura, Effect of scattering on intrinsic anomalous Hall effect investigated by Lorenz ratio, *Phys. Rev. B* **81**, 054414 (2010).
- [25] X. Li, L. Xu, L. Ding, J. Wang, M. Shen, X. Lu, Z. Zhu, and K. Behnia, Anomalous Nernst and Righi-Leduc Effects in Mn_3Sn : Berry Curvature and Entropy Flow, *Phys. Rev. Lett.* **119**, 056601 (2017).
- [26] L. Xu, X. Li, X. Lu, C. Collignon, H. Fu, J. Koo, B. Fauqué, B. Yan, Z. Zhu, and K. Behnia, Finite-temperature violation of the anomalous transverse Wiedemann-Franz law, *Science Advances* **6**, eaaz3522 (2020).
- [27] G. Grissonnanche, A. Legros, S. Badoux, E. Lefrançois, V. Zlatko, M. Lizaire, F. Laliberté, A. Gourgout, J.-S. Zhou, S. Pyon, T. Takayama, H. Takagi, S. Ono, N. Doiron-Leyraud, and L. Taillefer, Giant thermal hall conductivity in the pseudogap phase of cuprate superconductors, *Nature* **571**, 376 (2019).
- [28] M. Hirschberger, J. W. Krizan, R. J. Cava, and N. P. Ong, Large thermal Hall conductivity of neutral spin excitations in a frustrated quantum magnet, *Science* **348**, 106 (2015).
- [29] Y. Onose, T. Ideue, H. Katsura, Y. Shiomi, N. Nagaosa, and Y. Tokura, Observation of the Magnon Hall Effect, *Science* **329**, 297 (2010).
- [30] C. Strohm, G. L. J. A. Rikken, and P. Wyder, Phenomenological evidence for the phonon hall effect, *Phys. Rev. Lett.* **95**, 155901 (2005).
- [31] L. Sheng, D. N. Sheng, and C. S. Ting, Theory of the phonon hall effect in paramagnetic dielectrics, *Phys. Rev. Lett.* **96**, 155901 (2006).
- [32] Y. Kagan and L. A. Maksimov, Anomalous hall effect for the phonon heat conductivity in paramagnetic dielectrics, *Phys. Rev. Lett.* **100**, 145902 (2008).
- [33] M. Mori, A. Spencer-Smith, O. P. Sushkov, and S. Maekawa, Origin of the phonon hall effect in rare-earth garnets, *Phys. Rev. Lett.* **113**, 265901 (2014).
- [34] G. Zheng, Z. Chen, C. Tan, M. Wang, X. Zhu, S. Albarakati, M. Algarni, J. Partridge, L. Farrar, J. Zhou, W. Ning, M. Tian, M. S. Fuhrer, and L. Wang, Gate-controllable giant anomalous Hall effect from flat bands in kagome metal CsV_3Sb_5 nanoflakes (2021), arXiv:2109.12588 [cond-mat.mtrl-sci].
- [35] K. Behnia, The nernst effect and the boundaries of the fermi liquid picture,

- Journal of Physics: Condensed Matter **21**, 113101 (2009).
- [36] J. H. Kim, J.-S. Rhyee, and Y. S. Kwon, Magnon gap formation and charge density wave effect on thermoelectric properties in the SmNiC₂ compound, Phys. Rev. B **86**, 235101 (2012).
- [37] Y. K. Kuo, K. M. Sivakumar, T. H. Su, and C. S. Lue, Phase transitions in Lu₂Ir₃Si₅: An experimental investigation by transport measurements, Phys. Rev. B **74**, 045115 (2006).
- [38] R. Gumeniuk, K. O. Kvashnina, W. Schnelle, A. Leithe-Jasper, and Y. Grin, Magnetic and transport properties of structural variants of Remeika phases: Th₃Ir₄Ge₁₃ and U₃Ir₄Ge₁₃, Phys. Rev. B **91**, 094110 (2015).
- [39] C. N. Kuo, R. Y. Huang, Y. K. Kuo, and C. S. Lue, Transport and thermal behavior of the charge density wave phase transition in CuTe, Phys. Rev. B **102**, 155137 (2020).
- [40] E. D. Kountz, J. Zhang, J. A. W. Straquadine, A. G. Singh, M. D. Bachmann, I. R. Fisher, S. A. Kivelson, and A. Kapitulnik, Anomalous thermal transport and strong violation of Wiedemann-Franz law in the critical regime of a charge density wave transition, Phys. Rev. B **104**, L241109 (2021).
- [41] H. Li, T. T. Zhang, T. Yilmaz, Y. Y. Pai, C. E. Marvinney, A. Said, Q. W. Yin, C. S. Gong, Z. J. Tu, E. Vescovo, C. S. Nelson, R. G. Moore, S. Murakami, H. C. Lei, H. N. Lee, B. J. Lawrie, and H. Miao, Observation of Unconventional Charge Density Wave without Acoustic Phonon Anomaly in Kagome Superconductors AV₃Sb₅ (A = Rb, Cs), Phys. Rev. X **11**, 031050 (2021).
- [42] Z. X. Wang, Q. Wu, Q. W. Yin, C. S. Gong, Z. J. Tu, T. Lin, Q. M. Liu, L. Y. Shi, S. J. Zhang, D. Wu, H. C. Lei, T. Dong, and N. L. Wang, Unconventional charge density wave and photoinduced lattice symmetry change in the kagome metal CsV₃Sb₅ probed by time-resolved spectroscopy, Phys. Rev. B **104**, 165110 (2021).
- [43] N. Ratcliff, L. Hallett, B. R. Ortiz, S. D. Wilson, and J. W. Harter, Coherent phonon spectroscopy and interlayer modulation of charge density wave order in the kagome metal CsV₃Sb₅, Phys. Rev. Materials **5**, L111801 (2021).
- [44] L. Nie, K. Sun, W. Ma, D. Song, L. Zheng, Z. Liang, P. Wu, F. Yu, J. Li, M. Shan, D. Zhao, S. Li, B. Kang, Z. Wu, Y. Zhou, K. Liu, Z. Xiang, J. Ying, Z. Wang, T. Wu, and X. Chen, Charge-density-wave-driven electronic nematicity in a kagome superconductor, Nature **604**, 59 (2022).
- [45] L. Xu, X. Li, L. Ding, T. Chen, A. Sakai, B. Fauqué, S. Nakatsuji, Z. Zhu, and K. Behnia,

- Anomalous transverse response of Co_2MnGa and universality of the room-temperature $\alpha_{ij}^A/\sigma_{ij}^A$ ratio across topological magnets, *Phys. Rev. B* **101**, 180404 (2020).
- [46] D. Hou, G. Su, Y. Tian, X. Jin, S. A. Yang, and Q. Niu, Multivariable Scaling for the Anomalous Hall Effect, *Phys. Rev. Lett.* **114**, 217203 (2015).
- [47] Y. Gan, W. Xia, L. Zhang, K. Yang, X. Mi, A. Wang, Y. Chai, Y. Guo, X. Zhou, and M. He, Magneto-Seebeck effect and ambipolar Nernst effect in the CsV_3Sb_5 superconductor, *Phys. Rev. B* **104**, L180508 (2021).
- [48] J. Long, Phonon drag effects in tungsten below 2.6°K, *Physics Letters A* **25**, 677 (1967).
- [49] R. Bel, K. Behnia, and H. Berger, Ambipolar Nernst effect in NbSe_2 , *Phys. Rev. Lett.* **91**, 066602 (2003).
- [50] Zengwei Zhu and Huan Yang and Aritra Banerjee and Liam Malone and Benoît Fauqué and Kamran Behnia, Nernst quantum oscillations in bulk semi-metals, *Journal of Physics: Condensed Matter* **23**, 094204 (2011).
- [51] C. Li, X. Wu, H. Liu, C. Polley, Q. Guo, Y. Wang, X. Han, M. Dendzik, M. H. Berntsen, B. Thiagarajan, Y. Shi, A. P. Schnyder, and O. Tjernberg, Spectroscopic Evidence for a Three-Dimensional Charge Density Wave in Kagome Superconductor CsV_3Sb_5 (2021), arXiv:2112.06565 [cond-mat.str-el].
- [52] K. Nakayama, Y. Li, T. Kato, M. Liu, Z. Wang, T. Takahashi, Y. Yao, and T. Sato, Multiple energy scales and anisotropic energy gap in the charge-density-wave phase of the kagome superconductor CsV_3Sb_5 , *Phys. Rev. B* **104**, L161112 (2021).
- [53] R. Lou, A. Fedorov, Q. Yin, A. Kuibarov, Z. Tu, C. Gong, E. F. Schwier, B. Büchner, H. Lei, and S. Borisenko, Charge-Density-Wave-Induced Peak-Dip-Hump Structure and the Multiband Superconductivity in a Kagome Superconductor CsV_3Sb_5 , *Phys. Rev. Lett.* **128**, 036402 (2022).
- [54] Z. Liu, N. Zhao, Q. Yin, C. Gong, Z. Tu, M. Li, W. Song, Z. Liu, D. Shen, Y. Huang, K. Liu, H. Lei, and S. Wang, Charge-Density-Wave-Induced Bands Renormalization and Energy Gaps in a Kagome Superconductor RbV_3Sb_5 , *Phys. Rev. X* **11**, 041010 (2021).
- [55] T. M. McCormick, R. C. McKay, and N. Trivedi, Semiclassical theory of anomalous transport in type-ii topological weyl semimetals, *Phys. Rev. B* **96**, 235116 (2017).
- [56] Z. Wang, R. Boyack, and K. Levin, Heat-bath approach to anomalous thermal transport: effects of inelastic scattering, arXiv e-prints , arXiv:2112.13148 (2021),

arXiv:2112.13148 [cond-mat.mes-hall].

- [57] L. Ding, J. Koo, C. Yi, L. Xu, H. Zuo, M. Yang, Y. Shi, B. Yan, K. Behnia, and Z. Zhu, Quantum oscillations, magnetic breakdown and thermal Hall effect in $\text{Co}_3\text{Sn}_2\text{S}_2$, *Journal of Physics D: Applied Physics* **54**, 454003 (2021).